Using Breakdown Phenomenon As Mobile Magnetic Field Sensor in Microfluidics

Hugo Salmon, *Student Member, IEEE,* Laurent Couraud and Gilgueng Hwang, *Member, IEEE*

Abstract— Sensing magnetization and enhancing dynamics performances is essential while studying wireless magnetic mobile robots. Sensing physical parameters in microfluidic environments has strongly been demanded in various lab-on-a-chip applications as well. In this paper, we propose mobile microrobots as mobile sensor in microfluidics. We develop an original environment for high-resolution dynamic tracking and analysis in microfluidic chips. Studying robot dynamics in low Reynolds fluid with no magnetic sensor in the chip is challenging as the field distribution and robot magnetization are not well known. Our intended goal is to explore intrinsic magneto-fluidic sensing capacities to collect more information on the micro-system. We successfully integrate our robot into a transparent microfluidic chip for high-temporal resolution analysis of dynamics. We develop an electromagnetic setup allowing complete remote control (at low power $\lesssim 5mT$) of rotational behaviour. We study a breakdown phenomenon up to 1kHz signal and develop a scalar method analyzing rotational dynamics to enhance their sensing capacity.

I. INTRODUCTION

Using MEMS untethered micro-robots in fluids (microswimmers) as wireless manipulation tools has been developed widely with the intended goal to obtain in-vivo applications for biomedical [1-2], micromanipulation and/or cargo transport [3]. At micro/nanoscale, physics turns out to be quite different from macro-world and movements and/or regular operations remain quite challenging [4], low Reynolds number (with $R_e = \frac{\rho v L}{\mu} \ll 1$ being density ρ of fluid, v its speed, L a characteristic linear dimension and μ the dynamic viscosity) being much lower. Among other consequences - linearity, symmetry – as described in (1) by Stokes flow equation, a simplified version of Navier-Stokes:

$$\vec{\nabla} P = \mu \vec{\Delta}^2 \vec{u} + \vec{f} \qquad (1)$$

(where μ is the viscosity of the fluid, P its pressure, u its velocity & f is an applied body force), the system is overdamped [5]. Inertial effects and other body forces are then predominated by surface phenomenona, such as viscous drag, electrostatic forces or capillarity.

To perform swimming, several approaches are possible and have been explored. E. Coli Bacterium [5-7] because of its size and helical flagella, has the advantage of naturally fitting in-vivo environments but controlling their movement relies on complex processes such as chemotaxis [6] or biophysics phenomena [7], with a very limited control of movement for external users.

Some other works have focused on developing hybrid swimmers [8-9], combining metallic materials with living organisms. Thanks to the advances in microfabrications
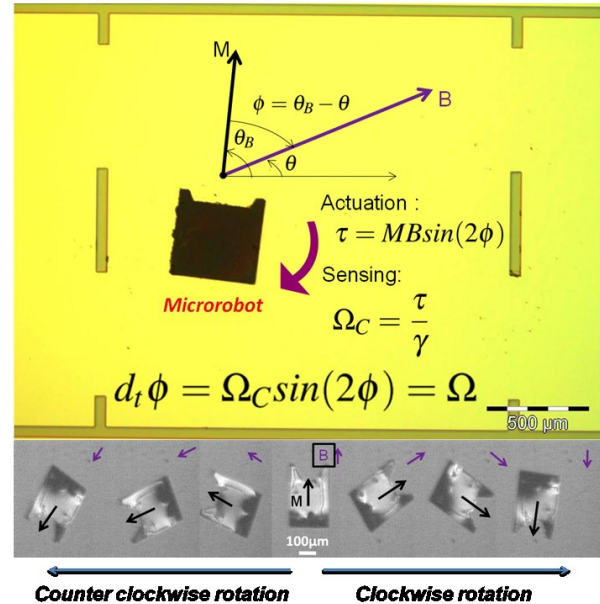

Figure 1. Top: capture of an example design of MagPole, schematic of actuating principle in damped environment & sensing at cut-off frequency; Below: Magnetization *M* tend to align to magnetic field B in any direction of the plan

and dynamic remote control with robotics, MEMS offer now a broad spectrum of development for purely artificial solutions [10], with a precise control over geometry, material and propulsion. Different particles have been designed, from nanobeads [3] to millimetric bodies [10]. Remote interaction has been achieved in dry and wet environment [11] using electrophoresis [12-13]or piezoelectric effects [14] but they require electrodes around the swimmer. Magnetic waves [15-19] have the advantage of generating a force and a torque over ferromagnetic corpses thanks to their magnetization without disturbing electrochemical equilibrium. To obtain higher D.O.F and faster time-response, using electromagnets controlled by digital-analog conversion should be considered rather than permanent magnets.

As it is difficult to know the field distribution of a magnetic device in microfluidics – due to confinement, oxidation and fabrication limitation, developing sensing capacities directly from the microswimmer is a major issue, needing to better understand dynamics i.e. magnetic forces at stake. We will see in section II it means determining local amplitude as well as field gradient. Finally, if knowing more about "what" is swimming and "how" is still of great interest, "where" has not been much explored. Environments such as microfluidic chip (lab-on-chip) [20] offer an adapted framework to study in-vitro applications and our goal here is to develop mobile

magnetic field sensor adapted to such microfluidic devices. We propose and extend our recently developed ferromagnetic micromobile robots named MagPol [21] for its capacity to POLarize MAGnetically– see Fig.1 pictures. It can enlarge the area of exploration in-vitro combining lab-on-chip and micro-robotics. It could open the way for in-vitro operations with broad applications for manipulation but also sensing, especially in harsh and inaccessible environment like liquid with toxicity or wide thermodynamic conditions. We have recently demonstrated full-planar motion and ability to polarize and manipulate micro-objects in microfluidics with an original strategy. We here focus exclusively on its dynamics to demonstrate its ability as a magnetic transducer (sensor and actuator). Though low Reynolds number induce a heavily damped environment, it can also become with simpler physics as a measuring tool for its environment, using an optical or magnetic torque momentum [22]. The magnetic field sensing is based on monitoring the cut-off frequency and the speed of the microrobot while their rotation and translational motion by external rotating magnetic field. The advantage of using MagPol is demonstrating high dynamics and control in both rotational and translational motions in such confined microfluidic environments, enhancing the magnetic field sensing temporal resolution.

In this paper, we integrate our microrobot in an original PDMS (polydiméthylsiloxane)/Glass microfluidic chip and develop a specific chain of command for sensing capacities. After reminding in section 2 the principles of Adler theory [23] on the breakdown phenomenon studied, the system overview and its important role in transducing will be described in the section 3. We then compare in section 4 experimental results to model and demonstrate first qualitative and quantitative results on magnetization sensing. In the final section, we discuss the perspective of development of those sensing capacities and applications.

II. WIRELESS IMMERSED TRANSDUCING

Any torque τ applied on the vertical axis **z** of a particle in Stokes fluid, because of heavy damping, is directly related to the particle angular speed (we neglect the inertial term) in the differential equation (2)

$$\gamma d_t \theta + \tau = 0 \qquad (2)$$

where γ is the striction coefficient toward, θ is the angular position & d_t the derivative with respect to time.

If we generate a uniform magnetic field on a particle containing ferromagnetic material magnetized horizontally,

$$\vec{F} = (\vec{M}.\vec{\nabla})\vec{B} = \vec{0} \qquad (3)$$

$$\vec{\tau} = \vec{M} \wedge \vec{B} = MB\sin(2(\theta_B - \theta)) \qquad (4)$$

M being the magnetization of the ferromagnetic parts, θ_B the direction of the uniform field, it induces exclusively a torque – equation (4) - toward vertical axis, because of field uniformity and horizontal magnetization. The consequence is two position of equilibrium on the symmetry axis, one only being stable and the particle
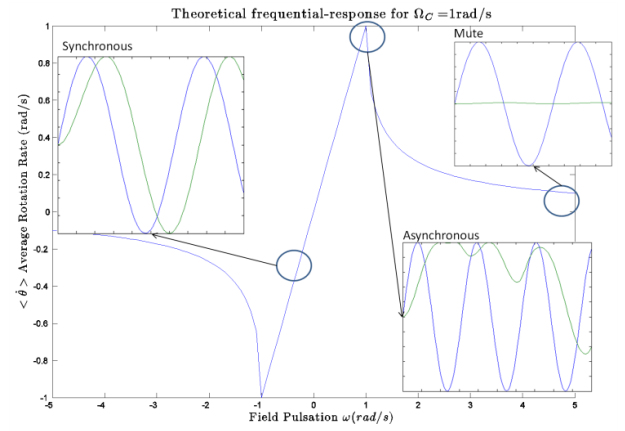

Figure 2. Average Rotation Rate from equation (2) - displaying breakdown phenomenon - and temporal responses simulated using ODE solver. Asymptotic frequency responses to rotating magnetic fields can be described by (6) & (7); each regime typical temporal response is illustrated by the cosine modulated angular phase of robot - in green – and B field in blue.

magnetic moment necessarily align toward the field axis – see Fig.1. Generating translation movements require a gradient distribution – equation (3), which can be delivered by a permanent magnet or an electromagnet controlled by electric current.

Under a rotating magnetic field toward vertical axis, if we name $\phi = \Omega t - \theta$ the rotating phase, it turns previous equation to simply:

$$d_t \phi + \Omega_C \sin(2\phi) = \Omega \qquad (5)$$

with a cut-off frequency $\Omega_C = \frac{MB}{\gamma_z}$, where M is the magnetization of the ferromagnetic layer of the robot, B the flux density of the field, Ω its pulsation and θ the particle angular position in horizontal plane. γ_z is the resistive coefficient due to fluid viscosity and substrate roughness and ϕ is the phase difference of the robot angular position with the field phase.

This parametric ordinary differential equation (5) has been previously described by Adler [23] as a quite complex behaviour with a breakdown phenomenon [22, 24-25] at Ω_C generating two different kinetic regimes [24] (6) and (7):

$$<\dot{\theta}> = \Omega \ for \ \Omega < \Omega_C \qquad (6)$$

$$<\dot{\theta}> = \Omega - \sqrt{\Omega^2 - \Omega_C{}^2} \ for \ \Omega \geq \Omega_C \qquad (7)$$

In synchronous regime, for $\Omega < \Omega_C$, the robot tends quickly to a constant rotating phase $\phi = \frac{1}{2} A\sin(\frac{\Omega}{\Omega_C})$. The problem of measuring it is it only gives a relative result: first steps of command (CPU & electronics) delay the actuation of the robot, inducing a constant error in $\Omega_{C,measured}$. At higher frequency $\approx 1 \ kHz$, the robot does not respond with our device maximal power and we consider the system as mute – Fig.2.

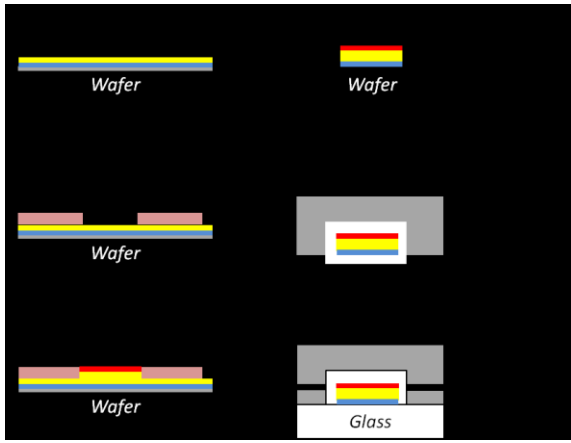With an offline tracking, the particle rotation can be

Figure 3: Fabrication of a mobile magnetic field sensor in PDMS/Glass Microfluidic; (a) - (d): robot fabrication; (e) & (f): fabrication of a PDMS microfluidic via channel and permanent bonding including the robot using plasma to seal fluidic chip, injection being possible on PDMS sides
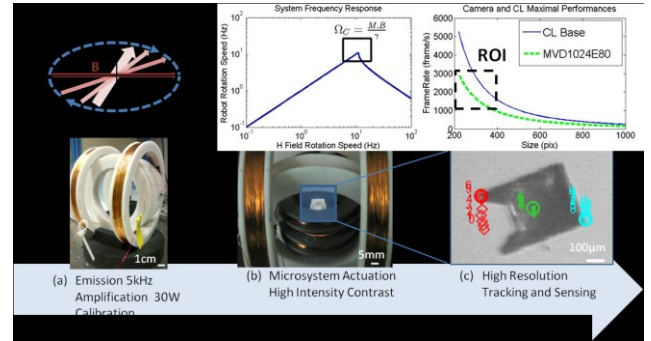

Figure 4: Schematic system oriented for magneto-fluidic sensing (a): (Bottom) Emission of magnetic field by electromagnetic circuit is controlled from a C# programmed GUI and, if not calibrated, generates an imperfectly circular magnetic flux (see Top) (b): (Top) Robot transfer function, highlighting how the system respond asymptotically to the transition (Bottom) All-transparent lab-on-chip integrating backlighting for high contrast and luminosity (c): (Top) Fast Camera temporal resolution function of CameraLink Configuration and a square frame size. Exposure time is fixed to its minimum (10μs). (Bottom) Tracking rotation through two distinct points of the robot.

simply determined in time by computing the angle formed by two distinct points of the robot (Fig.4 c) after measure. We can determine a value of Ω_C by an experimental fitting to the asymptotic behaviour giving us an equation relating fluidic and robots geometry parameters (from striction coefficient) to magnetic inputs.

III. SYSTEM

A. Microrobot design

The swimming MEMS consists – see Fig. 1 pictures of 2 different planar geometry - of a 2 μm Au and a 5 μm Ni ferromagnetic layer grown with usual bottom-up techniques, including lithography and electroplating on a Ti/Ni substrate – see Fig.3. The important proportion of ferromagnetic material allows it to reach higher magnetization, developing a stronger torque i.e. a higher cut-off frequency Ω_C.

The magnetization depending on robot symmetry, its design - as seen on Fig.1 pictures - defines clearly one horizontal axis toward the arms and has the advantage of being simple enough for tracking rotational phase ϕ .

It is included in a microfluidic chamber with depth of 320μm.The transparency of the whole chip is a critical choice for imaging and tracking quality, as we will detail in the III.D section. We used a polished glass wafer as the substrate combined to PDMS, a very common polymer in microfluidics. We insert needles in PDMS walls to generate flows in the chip and renew the solution.

PDMS having an important surface energy, it induces a high adsorption and we limit its use to the channels wall. It avoids the robot to get absorbed, in particular during the bonding phase where the surfaces of chip and the robot are ionized.

B. System oriented for magneto-fluidic sensing

In Fig.4(a) we input, amplify and emit a defined range of frequency including the cut-off frequency at a sub-millisecond ($200\mu s$) resolution. The micro-system described previously - see Fig.4(b) - respond to it almost instantaneously (as our design has low electromagnetic inertial effects) and a breakdown phenomenon is then observed. Fig.4(c) phase achieves the sensing and has directly a critical impact on the measure.

We developed a C program treating simultaneously signals emission and high-throughput data acquisition. Magnetic Coils were voltage-controlled through a data acquisition card (Sensoray® S626, 5kHz sampling frequency) and amplified through Servomotor controller (Maxon Motor® LSC 30/2,50W power |V |<10 and I < 2). Two types of magnetic setups have been utilized. The Helmholtz device induces exclusively uniform field on each axis X,Y or Z. By linear combination, it can generate a uniform in any direction with a maximum 5mT amplitude (over Ni coercitivity).

For a same voltage input, fabrication and assembly imperfections imply a different magnetic output toward two different axes. The consequence, as suggest Fig.4 (a), is an ellipticity of the rotational field. To conserve a uniform movement, a calibration is necessary. We use the robot angular position in function of two horizontal orthogonal field to obtain a calibration.

C. Magnetic Experimental Platform

Based on Helmoltz principle (inter-coils distance = coil radius), our coils generate a uniform magnetic field distribution. Magnetic experimental platforms were designed and optimized using Comsol and Matlab with FEM (Finite Element Method) and linear optimization to determine the optimal parameters: wire number of turns, material permeability and geometry. To measure a sufficiently wide range of cut-off frequency, dependent of
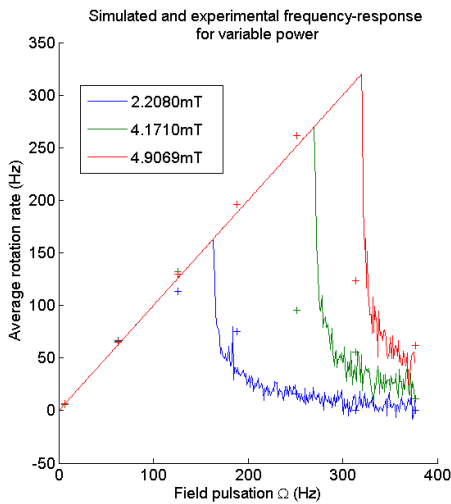
Figure 5: Comparison of simulated solutions (Runge-Kutta method) in continuous line and experimental (with tracking) frequency- response marked point for three different rotating magnetic fields

magnetic flux density amplitude, we need to transfer as much magnetic power as possible minimizing source-robot distance and maximizing coils' current volume. Polymer supports were fabricated with a three-dimensional additive manufacturer.To confirm the previous hypothesis of purely rotational movement, one other challenge is to contain the chip in a domain where the field is actually uniform (with less than a 5% global variation). We determined it comparing our simulation to a measure with a Hall effect sensor and made our chips fit it in the defined region.

D. Optics

As magnetic devices are too big or lenses working distance is too small to be included in standard microscope, we used a Navitar® zoom lens on top of the setup adapted for our study requirements. Attached on a manually controllable 6 DOF optical arm, it is possible to position anywhere without being in contact with any of the coils or sample.

Lighting is achieved either directly from the Navitar® lens with an included semi-reflecting mirror or from the bottom by an optical fiber source. If top-lighting can be an advantage because directly done from the lens, we observe a much better contrast and intensity in the second configuration. Moreover, as the light is transmitted and not reflected from the robot, it avoids instability of the robot texture during tracking. As fast frame-rate (>5 kframe/s) and tracking require respectively high intensity (exposure<ms) and steady high contrast, backlighting is highly recommended for a fine measurement.

E. Fast Imaging & Tracking

We used a Photonfocus® fast frame-rate camera directly connected via Camera Link protocol (allowing a maximum rate of 255 GBytes/s in BASE configuration). CL protocol is one of the fastest way to obtain directly to the computer such a high framerate and CMOS Camera usually work with it. Obtaining higher framerate is

possible only using embarked cameras with their own RAM and cooling system. It is not necessary for the dynamics we observe and it is a completely different budget. As we can see on Fig.4 (c) graph, camera performances (in green) in term of frame rate are necessary lower than Camera Link limitations. The frame rate t_{frame}, mainly depending of the exposure time and readout time, is the inverse of the frame time. The minimum frame time is calculated in sequential mode at constant framerate by:

$$t_{frame} = t_{exp} + t_{ReadOut} + t_{proc} + t_{RAM} \qquad (8)$$

where times on the right side of (8) are respectively exposure, readout, processing and RAM (Random Access Memory).As we can neglect processing and RAM refreshing time, depending of the computer performances -supposedly sufficient, it depends on exposure (>*10µs*) and readout time - directly related to the frame size. Acquisition are stocked on a direct memory allocation then converted in video and post treated using Tracker® open-source code. Two-points tracking allows extracting the angular phase from the visual data and identifying the breakdown phenomenon with a precision of the size of a pixel (~ 1-10 microns).

IV. SENSING DEMONSTRATION

To quickly demonstrate sensing capacity, we experiment with low temporal resolution (60Hz step) the variations of Magnetic flux and deduce a first qualitative result on the Magnetization of microrobot MagPol.

A. Uniform field sensing experimental demonstration

Protocol: we used the same chip/robot couple for all this study and realized it in isopropanol (IPA) at same concentration. We positioned it at the centre of the chip and magnetized it to saturation by putting in contact to the chip to a 1T permanent magnet (> Ni saturation magnetization). We generated the planar circular rotating field with a frequency varying from 1 to 400Hz with a 60Hz step. We input three different voltages, inducing a up-to 5mT magnetic flux. We can analyze dynamics with up-to 10 images per revolution at maximal frequency. We then integrate the signal to obtain an average rotation. We repeated the study for three different power input (calibrated i.e. no ellipticity). The post-treatment of recorded sequences is done using a tracking detecting robot shape and measuring angular variation between each frame.

Observation: The frequency-responses simulated on Matlab fits the experiment in the microfluidic chip on Fig.5, with what seems already to be a proportional dependency between magnetic power and cut-off frequency. If we define sensibility of the system as the variation of Ω_C depending on the power, we obtain an experimental value of 8.081 rad/(s.mT).
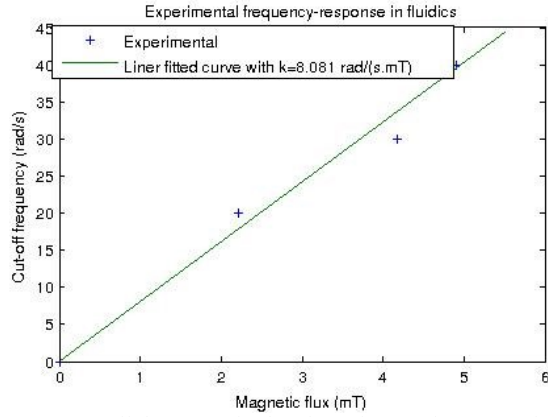
We observe in Fig. 6 the experiment fit the response to

Figure 6. Cut-off frequency in function of a rotating magnetic field amplitude, with linear fitting using least-square methodseveral powers a linear response giving us the ratio between magnetization and viscosity ratio and confirming the material was magnetized. As we treated exclusively the magnetized case which is linear, few points are necessary to determine the coefficient of the line.Nickel being a soft ferromagnetic material of known initial susceptibility χ_i=109 (unitless), coercitivity H$_c$=2mT and saturation M_{sat}=0.48 10^6A/m [26], we expect the two extreme cases:

$$\begin{cases} M \sim \dfrac{\chi_i B}{\mu_0} \ if \ initially \ non-magnetized \ robot \ (9) \\ M \sim M_{sat} \ if \ initially \ magnetized \ robot \quad (10) \end{cases}$$

where μ_0 is vacuum permeability ($\neq \mu$ the fluid viscosity). First qualitative result is the confirmation from Fig. 6 that the robot remains magnetized, the cut-off frequency being directly proportional to the magnetic flux $\Omega_C = \dfrac{M_{sat}B}{\gamma_z}$. A non-magnetized or demagnetized (possible, due to low coercitivity) robot would have had a quadratic variation with the information that allows, as the Ni saturation value is typically 0.48A/m at ambient temperature, to approximate the value of the damping coefficient.

B. Gradient field dynamics

Protocole: We induced a gradient distribution using a dome containing 4 electromagnets on orthogonal axes and sharing a common center. Being able to generate a force in any direction of the plane by linear superposition of the axes gradients, we can achieve a movement with up-to 30mT amplitude of field and 3mT/cm gradient, position it anywhere and analyze its dynamics at high framerate using a tracking algorithm. A 0.8V step input on an arbitrary axis generates a gradient magnetic field constant in time. We can then compare to the dynamics predicted by our approximation.

TABLE I. EXPERIMENTS PARAMETERS, FORCE INVOLVED AND R$_E$

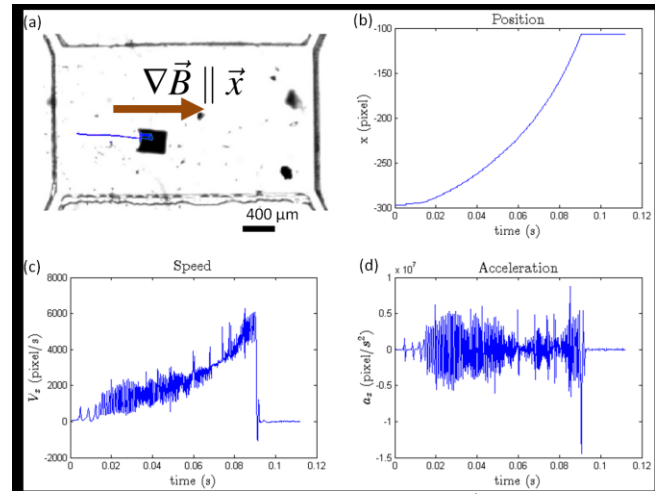| m_{Robot} ng	μ cP	r μm	β kg.s/m	a_{max} m/s^2	V_{max} m/s	F_{drag} nN	$m.a_x$ pN	R_e
3.56	1.96	250	9.24e-6	58.5	0.07	648	21	10^{-2}

Figure 7. (a) Translational motion dynamics by $\nabla\vec{B}$ gradient magnetic field induced with a 0.8 V input on a single axis $\vec{x}$. High temporal resolution (here 6600 frame/s) allows by tracking the robot position (b) to reach the speed values (c) and obtain a range of the force applied on the microrobot through acceleration (d). 3mm translation in 90ms with a constant in time input in backward motion. 1pixel~11.7μm

Observation: Microrobot, with a high proportion of ferromagnetic part, *can reach high-speed – Fig.7(b). At maximum speed, we* reach the limit *(10^{-2}) of low Reynolds* fluid. Striction makes it difficult to control *at low-speed too. It requires a* high-temporal res*olution as well as a sufficient* resolution of field amplitude, i.e. voltage input. We obtain with a sub-millisecond resolution the translational motion dynamics - Fig. 7 - on axis $\vec{x}$ in the position y.

Supposing at low power we are still in Low Reynolds approximation as in Section II, magnetic torque is directly related to the viscosity & microrobot speed

$$m_{\overline{robot}}\cdot a_x + M_{sat}\nabla B - \beta V_x = 0 \qquad (7)$$

where $\beta = 6\pi\mu r$ is the Stokes drag coefficient, a_x acceleration, V_x acceleration, μ IPA viscosity at 25°C and r Stokes radius (radius of a sphere containing the robot). We used Fig.7 data to complete Table I. We deduced the Forces at stake and R$_e$, justifying we can neglect inertia term for Eq. (7). Varying the power input and y position, we can determine a complementary scalar relation between magnetic gradient distribution and hydrodynamics.

V. CONCLUSION

A. Sensing Applications

Our system has demonstrated ability to determine the magnetization of the robot - see performances in Table II.

TABLE II. MAGNETO-FLUIDIC SENSING APPLICATIONS OF MEASURING Ω_C

B range	Bandwidth	Q	Sensitivity Hz/mT	Spatial / Time resolution
5mT	*0-500Hz*	1-1.4	8.081	500μm / 200μs

It can act as well - Table III - as a calibration tool for magnetic rotating field or a sensor of local viscosity of the fluid, the spatial resolution being the range of its in-plane

dimensions. It also provides, see Table III, an interesting tool for microswimmers development and microfluidics. It provides a scalar criterion which, depending on fixedparameters, determining experimentally an unknown variable. We can determine best geometries and environment for rotational motion and know more about the fluidic environment. This is given by $\gamma_z = \kappa \nu V$ if we suppose the drag coefficient γ_z directly proportional to the volume V of the robot and the fluid viscosity ν, the shape factor κ of the artificial swimmer.

TABLE III.   MAGNETO-FLUIDIC SENSING APPLICATIONS OF MEASURING Ω_C

Constants	Variable	Applications
M, B, ν and V	κ	Robot Optimization
M, B, κ and V	ν	Sensing Environment
B or M, κ, μ and V	M or B	

B. Future prospect

Transducing capacities (sensor as well as actuator) of MagPol in microfluidic chip have been compared to theory and confirmed. The system resolution is limited in power by the earth magnetic field and electromagnetic interferences, but a Faraday cage could increase it. Real-time sensing of the angular position could be achieved using an optimized tracking algorithm. It would simplify the long data treatment required by offline tracking. We could also extend the analysis by extracting more information from the excitable state by perturbing the input signals [25], obtaining more information about borders position. To control the position of the robot, adding complementary electromagnets - inducing magnetic gradient i.e. force – see Eq. (3) - to the Helmoltz setup controlling horizontal axes might be considered. Moreover, we now understand more the simple case of a uniform distribution but the more general case of gradient field distribution generate a translation movement in the direction of the magnetic dipole that is also damped, which means the speed is directly proportional to the power input. With an adapted tracking and model – see Fig.7, we could enlarge this study.

ACKNOWLEDGMENT

REFERENCES:

[1] M. Hofmann-Amtenbrink, B. von Rechenberg and H. Hofmann, "Superparamagnetic nanoparticles for biomedical applications" in Nanostructured Materials for Biomedical Applications, 2009, pp 119-149.

[2] Jordan, R. Scholz, P. Wust, H. Fahling and R. Felix, "Magnetic fluid hyperthermia (MFH): Cancer treatment with AC magnetic field induced excitation of biocompatible superparamagnetic nanoparticles" in Journal of Magnetism and Magnetic Materials, 201, 1999, pp 413-419.

[3] C. Gosse and V. Croquette, "Magnetic Tweezers: Micromanipulation and Force Measurement at the Molecular Level" in Biophysical Journal vol. 82 issue 6, June 2002.

[4] M. Purcell, "Life at low Reynolds" (American Institute of Physics) in. AIP Conf. Proc. 28, pp. 49-64, 1977.

[5] Guyon, J.-P. Hulin and L. Petit, "Hydrodynamique Physique" in CNRS Edition, 2001.

[6] Y. Sowa1, A.D. Rowe, M.C. Leake, T. Yakushi, M. Homma, A. Ishijima and R. M. Berry, "Direct observation of steps in rotation of the bacterial flagellar motor" in Nature 437, 2005, pp. 916-919.

[7] H.C. Berg and D.A. Brown, "Chemotaxis in Escherichia coli analysed by Three-dimensional Tracking" in Nature 239, 1972

[8] S. Chattopadhyay, R. Moldovan, C. Yeung and X. L. Wu, "Swimming efficiency of bacterium Escherichia coli in Proceedings of the National Academy of Science of the United States of America (PNAS), vol. 103, 2006, pp. 13712-13717.

[9] S. Martel, M. Mohammadi, O. Felfoul, Z. Lu and P. Pouponneau, "Flagellated Magnetotactic Bacteria as Controlled MRItrackable Propulsion and Steering Systems for Medical Nanorobots Operating in the Human Microvasculature" in IJRR 28 no.4, 2009, pp.571-582.

[10] J.J. Abbott, K.E. Peyer, M. C. Lagomarsino, L. Zhang, L. Dong and B. J. Nelson, "How should Microrobots swim?" in IJRR 28 no.11-12, pp.1434-1447, Nov. 2009.

[11] T. Kawahara, F. Lin, Y. Yamanishi and F. Arai, "High performance magnetically driven microtools with ultrasonic vibration for biomedical innovations" in ICRA 2011, pp. 3453 - 3454.

[12] G. Hwang, S. Haliyo and S. Rgnier, "Remotely Powered Propulsion of Helical Nanobelts" in *Proceedings of Robotics: Science and Systems* VI, 2011

[13] S.T. Chang, V.N. Paunov, D.N. Petsev and O. D. Velev, "Remotely powered self-propelling particles and micropumps based on miniature diodes" in Nature Materials 6, 2007, pp. 235-240.

[14] I.A. Ivan, G. Hwang, J. Agnus, M. Rakotondrabe, N. Chaill and S. Rgnier, "An impulsive and space-dependant in-plane control of MagPieR: the magnetic and piezoelectric microrobot" in ICRA 2011, pp.102-108.

[15] D.R. Frutiger, K. Vollmers, B.E. Kratochvil, B.J. Nelson, "Small, Fast, and Under Control: Wireless Resonant Magnetic Micro-agents" in IJRR vol 29 no. 5, 2010, pp. 613-636.

[16] C. Pawashe, S. Floyd and M. Sitti, "Multiple magnetic microrobot control using electrostatic anchoring" in Applied Physics Letters, vol.94, 2009, pp. 164-108.

[17] W. Mahoney, J. C. Sarrazin, E. Bamberg and J. J. Abbott,"Velocity Control with Gravity Compensation for Magnetic Helical Microswimmers" in Advanced Robotics 25 (2011) 10071028.

[18] A.F. Tabak and S Yesilyurt "Experiment-Based Kinematic Validation of Numeric Modeling and Simulated Control of an Untethered Biomimetic Microrobot in Channel"

[19] P. Tierno, R. Golestanian, I. Pagonabarraga and F. Sagus, "Controlled Swimming in Confined Fluids of Magnetically Actuated Colloidal Rotors" in Phys. Rev. Lett. vol 101 no.21, 2008.

[20] Y. Gao, A. van Reenen, M. A. Hulsen, A. M. De Jong, M. W. J. Prins and J. M. J. den Toonder, "Chaotic fluid mixing by alternating micro-particle topologies to enhance biochemical reactions" in µTAS 2012.

[21] H. Salmon, L. Couraud and G. Hwang, "Swimming Property Characterizations of Magnetic Polarizable" in IEEE International Conference on Robotics and Automation (ICRA), 2013.

[22] F. Pedaci, Z. Huang, M. v. Oene, S. Barland, N. H. Dekker, "Excitable Particles in an Optical Torque Wrench", Nature Physics vol. 7, pp 259-264, 2011.

[23] R. Adler "A study of locking phenomena in oscillators", Proc. IRE **34**, 351-357, 1946.

[24] B.H. McNaughton, K.A. Kehbein, J.N. Anker and R. Kopelman, "Sudden Breakdown in Linear Response of a Rotationally Driven Magnetic Microparticle and Application to Physical and Chemical Microsensing" in JPhysChem B vol 110 no. 38, pp 18958-18964.

[25] F. Pedaci, Z. Huang, M. van Oenu, S. Barland and N. H. Dekker, "Excitable particles in an optical torque wrench" in Nature Physics, 2010, pp 259-264.

[26] D. Jiles "Introdution to Magnetism and Magnetic Materials" in Chapman and Hall pp. 94-95.